

# Climate Affects Global Patterns Of Covid-19 Early Outbreak Dynamics

Gentile Francesco Ficetola<sup>1,2,\*</sup> & Diego Rubolini<sup>1\*</sup>

*1 Dipartimento di Scienze e Politiche Ambientali, Università degli Studi di Milano, via Celoria 26, I- 20133 Milano, Italy*

*2 Université Grenoble Alpes, CNRS, Université Savoie Mont Blanc, LECA, Laboratoire d'Ecologie Alpine, F-38000 Grenoble*

\*Contributed equally to this work; order was decided with a coin toss

Correspondence: francesco.ficetola@gmail.com, diego.rubolini@unimi.it

Phone numbers

Gentile Francesco Ficetola: 0039 338 1844255

Diego Rubolini: 0039 02 503 14718

1 Abstract

2

3 Environmental factors, including seasonal climatic variability, can strongly impact on spatio-  
4 temporal patterns of infectious disease outbreaks. We assessed the effects of temperature and  
5 humidity on the global patterns of COVID-19 early outbreak dynamics during January-March 2020.  
6 Climatic variables were the best drivers of global variation of confirmed COVID-19 cases growth  
7 rates. Growth rates peaked in temperate regions of the Northern Hemisphere with mean temperature  
8 of  $\sim 5^{\circ}\text{C}$  and humidity of  $\sim 0.6\text{-}1.0$  kPa during the outbreak month, while they decreased in warmer  
9 and colder regions. The strong relationship between local climate and COVID-19 growth rates  
10 suggests the possibility of seasonal variation in the spatial pattern of outbreaks, with temperate  
11 regions of the Southern Hemisphere becoming at particular risk of severe outbreaks during the next  
12 months.

13

14

15

16 A recently discovered coronavirus, SARS-CoV-2, is the aethiological agent of a pandemic disease,  
17 Covid-19, causing severe pneumonia outbreaks at the global scale<sup>1</sup>. Covid-19 cases are now  
18 reported in more than 155 countries and regions worldwide<sup>2</sup>. Three months after the discovery of  
19 SARS-CoV-2, the global pattern and the early dynamics of Covid-19 outbreaks seem highly  
20 variable. Some countries have been experiencing limited growth and spread of Covid-19 cases,  
21 while others are suffering widespread community transmission and nearly exponential growth of  
22 infections<sup>2</sup>. Given the impact of environmental conditions on the transmission of many pathogens,  
23 we tested the hypothesis that the severity of Covid-19 outbreaks across the globe is affected by  
24 spatial variation of key environmental factors, such as temperature, air humidity and pollution<sup>3-7</sup>.  
25 We then evaluated if this could help to illustrate global variation in the risk of severe Covid-19  
26 outbreaks in the coming months.

27 Relying on a publicly available global dataset<sup>2</sup>, we computed the daily growth rates  $r$  of  
28 confirmed Covid-19 cases (Covid-19 growth rate hereafter) for 121 countries/regions (see the  
29 Methods section and Table S6 in the Supplementary Appendix). We limited our measure of  
30 epidemics growth rate to the first 5 days after reaching a minimum threshold of confirmed cases  
31 (25, 50 or 100), as the mean incubation period of Covid-19 is ca. 5 days<sup>8</sup> and, immediately after the  
32 first confirmed cases, many countries put in place unprecedented containment measures to mitigate  
33 pathogen spread and community transmission<sup>9</sup>. Variation at these early epidemic growth rates  
34 should best reflect the impact of local environmental conditions on disease spread. We restricted  
35 analyses to data reported before March 19, as during that week many regions of the world adopted  
36 stringent containment measures even in absence of large numbers of reported cases. For instance,  
37 on March 17, 37 US states closed schools to prevent disease spread, including several states with  
38 less than 25 confirmed Covid-19 cases<sup>10</sup>. We also considered additional factors that could affect  
39 SARS-CoV-2 transmission dynamics, such as human population density, government per-capita  
40 health expenditure, and average air pollution levels (fine particulate matter; see Methods).

41 Covid-19 growth rates showed high variability at the global scale (Fig. 1A-C). The observed  
42 daily growth rate after reaching 50 cases ( $r_{50}$ ) was on average 0.18 [95% CI 0.16-0.19], and ranged  
43 from 0.01 (Kuwait) to 0.44 (Denmark). The highest growth rates were observed in temperate  
44 regions of the Northern Hemisphere (Fig. 1C). Growth rates calculated using different minimum  
45 thresholds of confirmed cases (25 or 100) were strongly positively correlated (see Methods),  
46 indicating robustness of our results to the choice of thresholds.

47 Climate variables were the most important predictors of Covid-19 growth rate (Table S1).  
48 The best-fitting linear mixed model suggested that  $r_{50}$  is non-linearly related to spatial variation in  
49 mean temperature of the outbreak month (Fig. 1A, Tables S2-S3). Growth rates peaked in regions  
50 with mean temperature of  $\sim 5^{\circ}\text{C}$  during the outbreak month, and decreased both in warmer and  
51 colder climates (Fig. A, Table S3). The comparison of models with different combinations of  
52 predictors confirmed temperature as the variable with the highest relative importance in explaining  
53 variation of  $r_{50}$  (Table S1), and temperature was the only parameter included in the best-fitting  
54 model (Tables S2-S3). Temperature and humidity of the outbreak month showed a strong, positive  
55 relationship across regions (Fig. S1), thus they could not be included as predictors in the same  
56 model. When we repeated the analyses including humidity instead of temperature,  $r_{50}$  varied  
57 significantly and non-linearly with humidity, peaking at  $\sim 0.6\text{-}1.0$  kPa (Fig. 1B, Tables S4-S5). The  
58 best model also showed slightly larger growth rates in countries with greater health expenditure  
59 (Table S5), possibly because of more efficient early reporting and/or faster diagnosis of Covid-19  
60 cases.

61 Results were highly consistent if we calculated growth rates after minimum thresholds of 25  
62 or 100 cases ( $r_{25}$  and  $r_{100}$ , respectively) instead of 50 (Tables S3 and S5). Human population density  
63 and air pollution showed very limited relative importance values (always  $< 0.50$ ; Table S1).

64 We then displayed potential seasonal changes in Covid-19 growth rates by projecting our  
65 best model of  $r_{50}$  in relation to temperature under the average temperature conditions of the current  
66 (March) and next (June and September) months (Fig. 1C-E). The predicted global distribution of  
67 Covid-19 growth rates based on March temperatures showed favorable conditions for disease  
68 spread in most temperate regions of the Northern Hemisphere, and matched well with the observed  
69 spatial distribution of Covid-19 growth rates during the January-March global outbreak (Fig. 1C).  
70 The expected seasonal rise in temperatures during the next months could result in less suitable  
71 conditions for Covid-19 spread in these areas. Conversely, seasonally decreasing temperatures  
72 could accelerate disease spread in large areas of the Southern Hemisphere, including south  
73 America, south Africa, eastern Australasia and New Zealand (Fig. 1D-E).

74 The management of Covid-19 outbreaks is undoubtedly one of the biggest challenges  
75 governments will face in the coming months. Our spatially-explicit analysis suggests that, at least in  
76 some parts of the world, ongoing containment efforts could benefit from the interplay between  
77 pathogen spread and local climate. We do not claim that climate is the single major driver of Covid-  
78 19 spread. The huge variation of Covid-19 growth rates among regions with similar climate indeed  
79 suggests that diverse and complex social and demographic factors, as well as stochasticity, may  
80 strongly contribute to determine the severity of Covid-19 outbreaks. Yet, climate can contribute to  
81 explain the variability in global patterns of Covid-19 growth rates. In the coming months, we may  
82 thus expect that large areas of the Southern Hemisphere will show environmental conditions  
83 promoting severe Covid-19 outbreaks.

84

## 85 **Materials and methods**

86

### 87 *Covid-19 dataset*

88 We downloaded the time series of confirmed Covid-19 cases from the Johns Hopkins University  
89 Center For Systems Science and Engineering (JHU-CSSE) GitHub repository

90 (<https://github.com/CSSEGISandData/Covid-19>; file 'time\_series\_19-covid-Confirmed.csv')<sup>11</sup>.

91 This datafile is updated once a day (at 23:59 UTC) and reports, for each day since January 22, 2020,  
92 all confirmed Covid-19 cases at the country level or at the level of significant geographical units  
93 belonging to the same country, which we defined here as 'regions' (e.g. US states or China

94 provinces), whenever separate Covid-19 cases data for these regions are available. Initially, US data  
95 were reported by county but, as of March 9, they were reported at the state level. We therefore

96 merged all US county data before March 9 to state level, and used state-level time series for

97 subsequent calculations. With the exception of US data, in all other cases we maintained the

98 original country/region information adopted by the JHU-CSSE. The datafile considered for the

99 analyses was downloaded on March 19, 2020, and included confirmed Covid-19 cases until March

100 18, 2020. From this dataset, we selected data for all countries / regions for which local outbreaks

101 were detected. We define a local outbreak event when at least 50 positive cases were detected in a

102 given country / region, and calculated the growth rate of confirmed Covid-19 cases between day 1

103 and day 5, when day 1 was the day at which the 50 cases threshold was reached. We calculate the

104 daily growth rate  $r$  of confirmed Covid-19 cases for each country/region, assuming an exponential

105 growth as:  $r = [\ln(n \text{ cases}_{\text{day } 5}) - \ln(n \text{ cases}_{\text{day } 1})] / 5$ . We checked the robustness of our estimates of

106 growth rate by calculating daily growth rate after the first 25, 50 or 100 cases ( $r_{25}$ ,  $r_{50}$  and  $r_{100}$ ,

107 respectively). Growth rates estimated at different thresholds were strongly positively correlated

108 (Pearson's correlation coefficients,  $r_{25}$  vs.  $r_{50}$ :  $r = 0.74$ ;  $r_{50}$  vs.  $r_{100}$ :  $r = 0.81$ ).

109 The dataset does not report information on containment measures, and these may be highly

110 heterogeneous among countries/regions. We decided to calculate growth rate on the basis of the

111 first five days, in order to obtain an estimate of the non-intervened spread of the disease (i.e. before  
112 stringent containment measures are undertaken). Five days provides a reasonable trade-off between  
113 having to unreliable estimates of growth rates (if calculated on the basis of a smaller number of  
114 days, e.g. 3), and obtaining growth rates influenced by the enforcement of heavy containment  
115 measures (such as immediate isolation of confirmed cases). Five days is the median estimated time  
116 spanning before the onset of symptoms<sup>8</sup>, implying that infected patients might spread the virus for  
117 5 days undetected in absence of preventive control measures. The mean estimated growth rate of  
118 confirmed Covid-19 cases showed a tendency to decrease from  $r_{25}$  to  $r_{100}$  (mean and 95% c.i.:  $r_{25} =$   
119  $0.21 [0.19-0.22, n = 121]$ ,  $r_{50} = 0.18 [0.16-0.19, n = 90]$ ,  $r_{100} = 0.16 [0.14-0.18, n = 69]$ ), possibly  
120 because of the progressive effect of containment measures that were adopted in different countries  
121 at different times and different minimum thresholds after the onset of the local outbreak. We  
122 excluded from analyses countries/regions with less than 100000 inhabitants (in our dataset, San  
123 Marino only). As of March 19, 2020, the JHU-CSSE dataset provided information for a total of 121  
124 countries/regions for the calculation of  $r_{25}$ , 90 for  $r_{50}$ , and 69 for  $r_{100}$ . The final list of  
125 countries/regions included in the analyses, together with estimated confirmed Covid-19 growth  
126 rates at different thresholds, is reported in Table S6.

127

#### 128 *Environmental and socio-economic variables*

129 We considered two climatic variables that are known to affect the spread of viruses: mean air  
130 temperature and vapor pressure, which is a measure of absolute humidity. Previous studies showed  
131 that, for coronaviruses and influenza viruses, survival is generally higher at low temperature and  
132 low values of absolute humidity<sup>5,6,12-14</sup>. For each country/region, we thus calculated the mean  
133 monthly values for temperature (°C) and vapor pressure (kPa) for January, February and March on  
134 the basis of the WorldClim 2.1 raster layers at 10 arc-minutes resolution<sup>15</sup>. We relied on  
135 WorldClim climatic data because homogeneous data on conditions for the period January-March  
136 2020 are not yet available at a global scale (see e.g.

137 <https://www.ecmwf.int/en/forecasts/datasets/reanalysis-datasets/era5>), and spatial variation among  
138 areas of the world is generally much stronger than inter-annual variation for the same region<sup>16</sup>. As  
139 additional predictors, we considered mean human population density<sup>17</sup> (population density  
140 hereafter, expressed in inhabitants/km<sup>2</sup>) and per-capita government health expenditure (health  
141 expenditure hereafter) (indicator ‘Domestic General Government Health Expenditure (GGHE-D)  
142 per Capita in US\$; average of 2015-2017 values downloaded from the World Health Organization  
143 database at <https://apps.who.int/nha/database>). Health expenditure was available at country-level  
144 only: hence, regions within countries were assigned the same health expenditure value. Finally, it  
145 has been proposed that air pollution, and especially fine atmospheric particulate, could enhance the  
146 persistence and transmission of coronaviruses<sup>3,18</sup>. We therefore extracted values of annual  
147 concentration ( $\mu\text{g}/\text{m}^3$ ) of ground-level fine particulate matter (PM2.5) for 2016 from the NASA  
148 Socioeconomic Data and Applications Center<sup>19</sup>, and calculated the mean abundance of PM2.5 for  
149 each country/region. We performed all spatial analyses using the raster package in R<sup>20</sup>.

150

### 151 *Statistical analyses*

152 We used linear mixed models (LMMs) to relate the global variation of  $r_{50}$ ,  $r_{25}$  and  $r_{100}$  to the five  
153 environmental predictors (temperature and humidity of outbreak month; population density; health  
154 expenditure and PM2.5). To associate climate variables to the estimated  $r$ -values for each  
155 country/region, we first extracted the mean month of the 5 days over which we computed the  $r$ -  
156 values (rounded to the nearest integer) (outbreak month). We then assigned to the  $r$ -values of each  
157 country/region the mean temperature and humidity of the month during which the outbreak  
158 occurred. Country was included as a random factor to take into account potential non-independence  
159 of growth rates from regions belonging to the same country. Non-linear relationships between  
160 climatic factors and ecological variables are frequent<sup>21</sup>, and in exploratory plots we detected a clear  
161 non-linear relationship between  $r$ -values and climate. Therefore, for climatic variables, we included



162 in models both linear and quadratic terms. Humidity, population density, health expenditure and  
163 PM2.5 were log<sub>10</sub>-transformed to reduce skewness and improve normality of model residuals.

164 We adopted a model selection approach to identify the variables most likely to affect the  
165 global variation of Covid-19 growth rate<sup>22</sup>. We built models representing the different  
166 combinations of independent variables, and ranked them on the basis of Akaike's Information  
167 Criterion (AIC). AIC trades-off explanatory power vs. number of predictors; parsimonious models  
168 explaining more variation have the lowest AIC values and are considered to be the "best models"<sup>22</sup>.  
169 For each candidate model, we calculated the Akaike weight  $\omega_i$ , representing the probability of the model given the data  
170<sup>23</sup>. We then calculated the relative variable importance of each variable (RVI) as the sum of  $\omega_i$  of the models where  
171 each variable is included. RVI can be interpreted the probability that a variable should be included in the best model  
172<sup>22,24</sup>. Model selection analyses and the calculation of RVI can be heavily affected by collinearity among variables. In our  
173 dataset, temperature and humidity showed a very strong positive correlation (Fig. S1 and Table S7); furthermore,  
174 population density was strongly positively associated with PM2.5 (Figure S1 and Table S7). Therefore, temperature and  
175 humidity, or population density and PM2.5, could not be considered together in the same models<sup>24,25</sup>. All other  
176 predictors showed weak correlations and should not cause collinearity issues<sup>25</sup> (Table S7). We therefore repeated the  
177 model selection for different combinations of uncorrelated variables. First, we considered temperature, health  
178 expenditure and population density as independent variables. Then we repeated the analysis using humidity instead of  
179 temperature, and we calculated the RVI of variables separately for these two model selection analyses. Finally, to assess  
180 the role of PM2.5, we repeated these two model selections analyses using PM2.5 instead of health expenditure. The  
181 RVI values for all tested models are reported in Table S1. Due to low RVI of PM2.5 in all models (Table S1), we  
182 subsequently report detailed results of models including population density instead of PM2.5 (Tables S2-S5). To test the  
183 robustness of our conclusion to subjective thresholds for the minimum number of cases, all analyses were repeated  
184 considering the three estimates of Covid-19 growth rate as dependent variables ( $r_{25}$ ,  $r_{50}$  and  $r_{100}$ ).

185 LMMs were fitted using the lmer function of the lme4 R package<sup>26</sup>, while tests statistics were calculated using  
186 the lmerTest package<sup>27</sup>. To confirm that spatial autocorrelation did not bias the outcome of our  
187 analyses, we calculated the spatial autocorrelation (Moran's  $I$ ) of the residuals of best-fitting models  
188 using the EcoGenetics package in R<sup>28</sup> at lags of 1000 km up to a maximum distance of 5000 km.  
189 Model residuals did not show significant spatial autocorrelation at any lag (in all cases, |Moran's  $I$  |

190 < 0.10 and  $P > 0.11$ ), suggesting that spatial autocorrelation was not a major issue in our analyses  
191 <sup>29</sup>.

192

## 193 References

194

- 195 1. World Health Organization. Coronavirus disease (COVID-2019) situation reports:  
196 <https://www.who.int/emergencies/diseases/novel-coronavirus-2019/situation-reports/> [accessed 1  
197 March 2020]; 2020.
- 198 2. Dong E, Du H, Gardner L. An interactive web-based dashboard to track COVID-19 in real  
199 time. *The Lancet Infectious Diseases* 2020;DOI:[https://doi.org/10.1016/S1473-3099\(20\)30120-1](https://doi.org/10.1016/S1473-3099(20)30120-1).  
200 Data available at <https://github.com/CSSEGISandData/COVID-19>.
- 201 3. Setti L, Passarini F, de Gennaro G, et al. Relazione circa l'effetto dell'inquinamento da  
202 particolato atmosferico e la diffusione di virus nella popolazione.  
203 [http://www.simaonlus.it/wpsima/wp-content/uploads/2020/03/COVID19\\_Position-](http://www.simaonlus.it/wpsima/wp-content/uploads/2020/03/COVID19_Position-Paper_Relazione-circa-l%E2%80%99effetto-dell%E2%80%99inquinamento-da-particolato-atmosferico-e-la-diffusione-di-virus-nella-popolazione.pdf)  
204 [Paper\\_Relazione-circa-l%E2%80%99effetto-dell%E2%80%99inquinamento-da-particolato-](http://www.simaonlus.it/wpsima/wp-content/uploads/2020/03/COVID19_Position-Paper_Relazione-circa-l%E2%80%99effetto-dell%E2%80%99inquinamento-da-particolato-atmosferico-e-la-diffusione-di-virus-nella-popolazione.pdf)  
205 [atmosferico-e-la-diffusione-di-virus-nella-popolazione.pdf](http://www.simaonlus.it/wpsima/wp-content/uploads/2020/03/COVID19_Position-Paper_Relazione-circa-l%E2%80%99effetto-dell%E2%80%99inquinamento-da-particolato-atmosferico-e-la-diffusione-di-virus-nella-popolazione.pdf): Società Italiana di Medicina  
206 Ambientale; 2020.
- 207 4. Sajadi MM, Habibzadeh P, Vintzileos A, Shokouhi S, Miralles-Wilhelm F, Amoroso A.  
208 Temperature and Latitude Analysis to Predict Potential Spread and Seasonality for COVID-19.  
209 2020:Available at SSRN: <https://ssrn.com/abstract=3550308>.
- 210 5. Kampf G, Todt D, Pfaender S, Steinmann E. Persistence of coronaviruses on inanimate  
211 surfaces and their inactivation with biocidal agents. *Journal of Hospital Infection* 2020;104:246-51.
- 212 6. Tamerius JD, Shaman J, Alonso WJ, et al. Environmental Predictors of Seasonal Influenza  
213 Epidemics across Temperate and Tropical Climates. *PLoS Pathog* 2013;9:12.

- 214 7. Wang J, Tang K, Feng K, Lv W. High Temperature and High Humidity Reduce the  
215 Transmission of COVID-19 (March 9, 2020). Available at SSRN  
216 2020:<http://dx.doi.org/10.2139/ssrn.3551767>
- 217 8. Li Q, Guan X, Wu P, et al. Early Transmission Dynamics in Wuhan, China, of Novel  
218 Coronavirus–Infected Pneumonia. *New England Journal of Medicine* 2020.
- 219 9. Hellewell J, Abbott S, Gimma A, et al. Feasibility of controlling COVID-19 outbreaks by  
220 isolation of cases and contacts. *The Lancet Global Health* 2020;8:e488-e96.
- 221 10. Maxouris C. These states have some of the most drastic restrictions to combat the spread of  
222 coronavirus. CNN 2020:[https://edition.cnn.com/2020/03/17/us/states-measures-coronavirus-](https://edition.cnn.com/2020/03/17/us/states-measures-coronavirus-spread/index.html)  
223 [spread/index.html](https://edition.cnn.com/2020/03/17/us/states-measures-coronavirus-spread/index.html).
- 224 11. Dong E, Du H, Gardner L. An interactive web-based dashboard to track COVID-19 in real  
225 time. *The Lancet Infectious Diseases* 2020.
- 226 12. Shaman J, Kohn M. Absolute humidity modulates influenza survival, transmission, and  
227 seasonality. *Proceedings of the National Academy of Sciences* 2009;106:3243.
- 228 13. Lowen AC, Steel J. Roles of Humidity and Temperature in Shaping Influenza Seasonality.  
229 *Journal of Virology* 2014;88:7692-5.
- 230 14. Lowen AC, Mubareka S, Steel J, Palese P. Influenza virus transmission is dependent on  
231 relative humidity and temperature. *PLoS Pathog* 2007;3:1470-6.
- 232 15. Fick SE, Hijmans RJ. WorldClim 2: new 1-km spatial resolution climate surfaces for global  
233 land areas. *Int J Climatol* 2017;37:4302-15.
- 234 16. Harris I, Jones PD, Osborn TJ, Lister DH. Updated high-resolution grids of monthly  
235 climatic observations – the CRU TS3.10 Dataset. *Int J Climatol* 2014;34:623-42.
- 236 17. Center for International Earth Science Information Network CCU. Gridded Population of  
237 the World, Version 4 (GPWv4): Population Density, Revision 11. Palisades, NY: NASA  
238 Socioeconomic Data and Applications Center (SEDAC); 2018.

- 239 18. van Doremalen N, Bushmaker T, Morris D, et al. Aerosol and surface stability of HCoV-19  
240 (SARS-CoV-2) compared to SARS-CoV-1. medRxiv 2020;2020.03.09.20033217:doi:  
241 <https://doi.org/10.1101/2020.03.09.20033217>.
- 242 19. van Donkelaar A, Martin A, Brauer M, et al. Global Annual PM2.5 Grids from MODIS,  
243 MISR and SeaWiFS Aerosol Optical Depth (AOD) with GWR, 1998-2016. Palisades NY: NASA  
244 Socioeconomic Data and Applications Center (SEDAC). <https://doi.org/10.7927/H4ZK5DQS>;  
245 2018.
- 246 20. Hijmans RJ. raster: Geographic data analysis and modeling. R package version 3.0-7:  
247 <http://CRAN.R-project.org/package=raster>; 2019.
- 248 21. Legendre P, Legendre L. Numerical Ecology. Amsterdam: Elsevier; 2012.
- 249 22. Burnham KP, Anderson DR. Model selection and multimodel inference: a practical  
250 information-theoretic approach. New York: Springer Verlag; 2002.
- 251 23. Lukacs PM, Thompson WL, Kendall WL, et al. Concerns regarding a call for pluralism of  
252 information theory and hypothesis testing. J Appl Ecol 2007;44:456-60.
- 253 24. Giam XL, Olden JD. Quantifying variable importance in a multimodel inference framework.  
254 Methods Ecol Evol 2016;7:388-97.
- 255 25. Dormann CF, Elith J, Bacher S, et al. Collinearity: a review of methods to deal with it and a  
256 simulation study evaluating their performance. Ecography 2013;36:27-46.
- 257 26. Bates D, Maechler M, Bolker BM, Walker S. Fitting Linear Mixed-Effects Models Using  
258 lme4. J Stat Softw 2015;67:1-48.
- 259 27. Kuznetsova A, Brockhoff B, Christensen HB. lmerTest Package: Tests in Linear Mixed  
260 Effects Models. J Stat Softw 2017;82:1-26.
- 261 28. Roser LG, Ferreyra LI, Saidman BO, Vilardi JC. EcoGenetics: An R package for the  
262 management and exploratory analysis of spatial data in landscape genetics. Mol Ecol Resour  
263 2017;17:e241-e50.

264 29. Beale CM, Lennon JJ, Yearsley JM, Brewer MJ, Elston DA. Regression analysis of spatial  
265 data. *Ecol Lett* 2010;13:246-64.

266

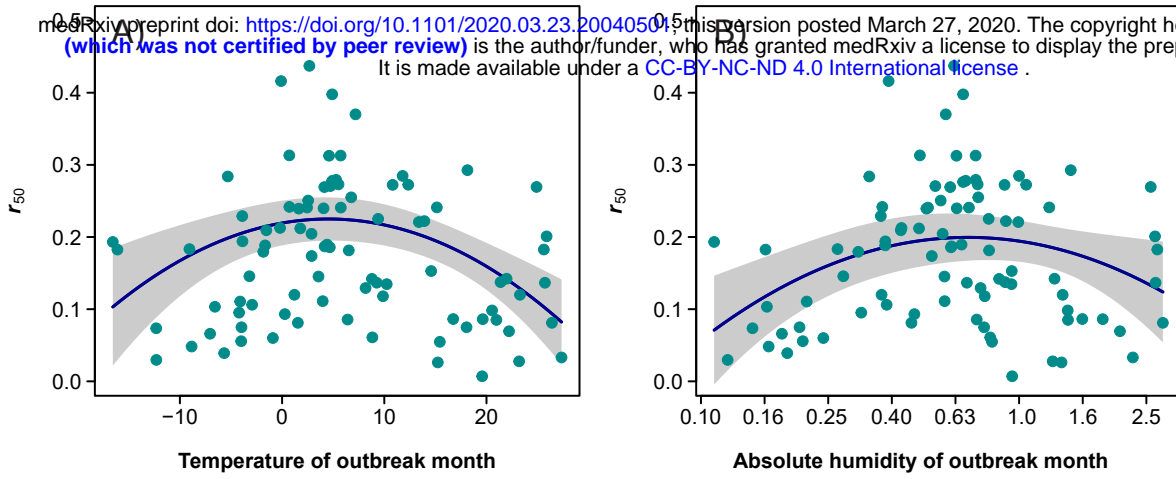
267

268 **Figure 1. Variation of Covid-19 growth rates in relation to climate, and spatial predictions for**  
269 **different months.**

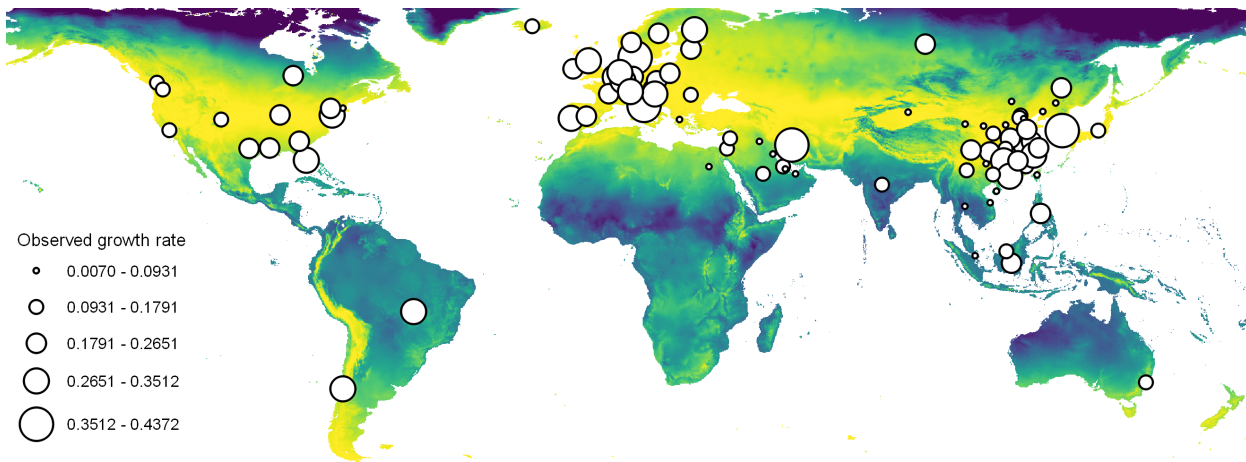
270

271 Variation of confirmed Covid-19 cases growth rates for the first 5 days after reaching a minimum  
272 threshold of 50 cases ( $r_{50}$ ) during the January-March 2020 pandemic outbreak ( $n = 90$   
273 countries/regions, see list in Table S6) in relation to the mean temperature (**Panel A**) and to the  
274 mean absolute humidity of the outbreak month (**Panel B**). The lines are obtained from the best-  
275 fitting linear mixed models (LMMs) of  $r_{50}$  in relation to temperature or humidity, respectively (see  
276 Tables S3 and S5). The quadratic terms of both temperature and humidity were highly significant  
277 (temperature:  $F_{1,87} = 14.4$ ,  $P < 0.001$ ; humidity:  $F_{1,84} = 7.82$ ,  $P = 0.006$ ; full details in Tables S3 and  
278 S5). Shaded areas are 95% confidence band. **Panel C** shows the global patterns of  $r_{50}$ , with the size  
279 of dots is proportional to the observed  $r_{50}$  value. The background shows the spatial prediction of  
280 growth rates according to mean March temperatures<sup>15</sup>. Predictions are based on the best-fitting  
281 LMM of  $r_{50}$  in relation to mean temperature of the outbreak month (Table S3). **Panels D and E**  
282 show the spatial prediction of growth rates according to mean June and September temperatures<sup>15</sup>,  
283 highlighting that optimal conditions for disease spread appear in temperate regions of the Southern  
284 Hemisphere.

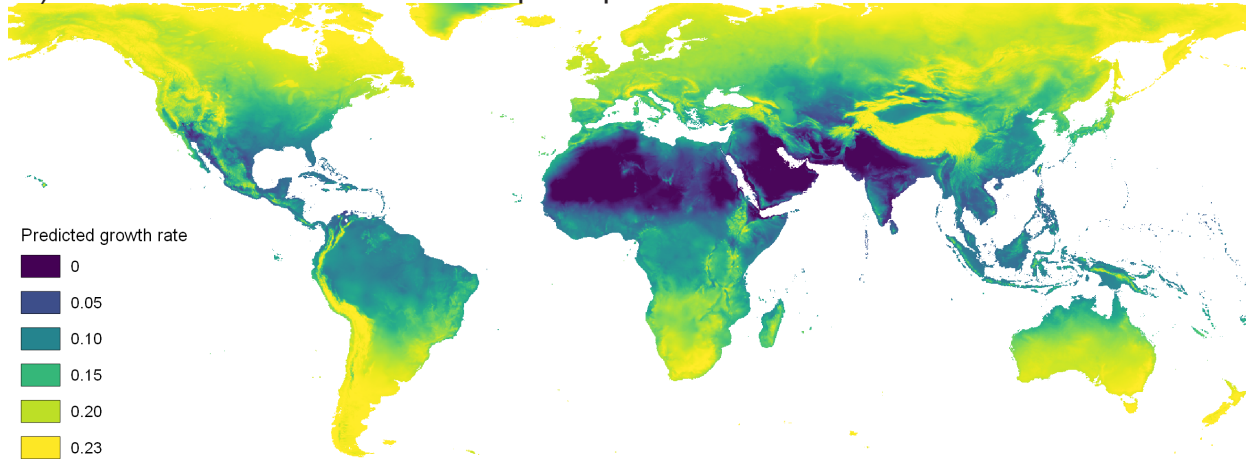
285



C) Observed growth rate, and spatial prediction for March



D) Spatial prediction for June



E) Spatial prediction for September

